On the Nature of Soft X-ray Weak Quasi-Stellar Objects

W. N. Brandt

Department of Astronomy and Astrophysics, 525 Davey Laboratory, Pennsylvania State University, University Park, PA 16802

A. Laor

Physics Department, Technion, Haifa 32000 Israel

Beverley J. Wills

Department of Astronomy, University of Texas at Austin, Austin, TX 78712

ABSTRACT

Recent studies of Quasi-Stellar Objects (QSOs) with *ROSAT* suggest the existence of a significant population of Soft X-ray Weak QSOs (SXW QSOs) where the soft X-ray flux is $\sim$ 10–30 times smaller than in typical QSOs. Why are these QSOs soft X-ray weak, and what is their relationship to Broad Absorption Line QSOs (BAL QSOs) and X-ray warm absorber QSOs? As a first step in a systematic study of these objects, we establish a well-defined sample of SXW QSOs which includes all $\alpha_{\rm ox} \leq -2$ QSOs from the Boroson & Green (1992) sample of 87 Bright Quasar Survey QSOs. SXW QSOs comprise $\approx 11\%$ of this optically selected QSO sample, and we find soft X-ray weakness in both radio-quiet and radio-loud QSOs. From an analysis of C IV absorption in the 55 BG92 QSOs with available C IV data, we find a remarkably strong correlation between $\alpha_{\rm ox}$ and the C IV absorption equivalent width. This correlation suggests that absorption is the primary cause of soft X-ray weakness in QSOs, and it reveals a continuum of absorption properties connecting unabsorbed QSOs, X-ray warm absorber QSOs, SXW QSOs and BAL QSOs. Many of our SXW QSOs have ultraviolet absorption that is intermediate in strength between that of X-ray warm absorber QSOs and that of BAL QSOs, and their X-ray absorption is also likely to be of intermediate strength. From a practical point of view, our correlation demonstrates that selection by soft X-ray weakness is an effective ($\gtrsim 80\%$ successful) and observationally inexpensive way to find low-redshift QSOs with strong and interesting ultraviolet absorption.

We have also identified several notable differences between the optical emission-line properties of SXW QSOs and those of the other Boroson & Green QSOs. SXW QSOs show systematically low [O III] luminosities as well as distinctive Hβ-line profiles. They tend to lie toward the weak-[O III] end of Boroson & Green eigenvector 1, as do many low-ionization BAL QSOs. Unabsorbed Seyferts and QSOs with similar values of eigenvector 1 have been suggested to have extreme values of a primary physical parameter, perhaps mass accretion rate relative to the Eddington rate ($\dot{M}/\dot{M}_{\rm Edd}$). If these suggestions are correct, it is likely that SXW QSOs also tend to have generally high values of $\dot{M}/\dot{M}_{\rm Edd}$. Finally, we present and discuss correlations between $\alpha_{\rm ox}$ and other QSO observables after removal of the SXW QSOs.

Subject headings: galaxies: active – galaxies: nuclei – quasars: general – X-rays: galaxies.

1. Introduction

While X-ray emission appears to be a universal property of Quasi-Stellar Objects (QSOs; Avni & Tananbaum 1986, hereafter AT86), there is evidence for a significant population of soft X-ray weak QSOs (SXW QSOs; Elvis 1992; Laor et al. 1997a; Yuan et al. 1998). These comprise $\sim 10\%$ of the optically selected QSO population and have soft X-ray emission that is $\gtrsim 10$–30 times weaker than expected based on their continuum luminosities in other bands. In general, the cause of soft X-ray weakness has not been well established, and it could arise as a result of (1) intrinsic or intervening X-ray absorption, (2) an unusual underlying spectral energy distribution, or (3) extreme X-ray or optical variability.

In this paper, we investigate the X-ray, ultraviolet and optical properties of a well-defined sample of SXW QSOs. Our main goals are (1) to determine if soft X-ray weakness correlates with other observables, (2) to examine the relationship between SXW QSOs, Broad Absorption Line QSOs (BAL QSOs) and QSOs with X-ray warm absorbers, and (3) to determine the reason for the low apparent soft X-ray luminosities of SXW QSOs. Regarding the second goal, it is known that BAL QSOs are generally weak in the soft X-ray band (e.g., Green & Mathur 1996), but the fraction of SXW QSOs that are BAL QSOs is poorly determined at present. Our focus is on objects that are more luminous and distant than local Seyferts (e.g., Maiolino & Rieke 1995). Our work differs from that of Green (1998) in that we study a smaller number of objects that are substantially more extreme in terms of their soft X-ray weakness.

2. Soft X-ray Weak QSO Selection

We have selected our SXW QSOs from the Boroson & Green (1992; hereafter BG92) sample. This sample is composed of all 87 QSOs from the Bright Quasar Survey (BQS; Schmidt & Green 1983) with $z < 0.5$, and our intention is to perform a thorough analysis of all the SXW QSOs in this sample. The BQS consists of the broad-line active galaxies with dominant star-like nuclei to the survey limits: $B \lesssim 16.2$ and $U - B \lesssim -0.44$ (for Galactic latitudes greater than 30° and declinations above −10°). To these limits it is thought to be $\gtrsim 70\%$ complete at $z < 0.5$ (see Véron et al. 1999), and a large amount of high-quality and uniformly analyzed data are available for the BG92 QSOs. Since the BQS QSOs were optically selected, the BQS should not be *directly* biased with respect to the inclusion or exclusion of SXW QSOs. Possible *indirect* biases are, unfortunately, inescapable when using current large-area QSO surveys (see Goodrich 1997 and Krolik & Voit 1998 for examples of potentially relevant indirect biases).

Our selection method is based upon $\alpha_{\rm ox}$, the slope of a power law defined by the rest-frame flux densities at 3000 Å and 2 keV. That is, $\alpha_{\rm ox} = 0.372 \log(f_{2\ {\rm keV}}/f_{3000\ \text{Å}})$ where $f_{2\ {\rm keV}}$ and $f_{3000\ \text{Å}}$ are flux densities.[1] While $\alpha_{\rm ox}$ calculations for many of the BQS QSOs have been performed before (e.g., Tananbaum et al. 1986), these are not sufficient for our purposes as they miss many of the SXW QSOs that we study here. These objects were either not observed or not detected. In addition, comparison of our $\alpha_{\rm ox}$ values with earlier ones allows us to search for $\alpha_{\rm ox}$ variability; extreme X-ray or optical variability could cause a QSO to appear soft X-ray weak (e.g., see Figure 1 of Boller et al. 1997). We have therefore calculated our own $\alpha_{\rm ox}$ values for the 87 BG92 QSOs following the method in the next paragraph.

When possible we have determined the 3000 Å flux densities needed for $\alpha_{\rm ox}$ using the data from Neugebauer et al. (1987). For the 13 BG92 QSOs without such data, we calculated 3000 Å flux densities using data from De Bruyn & Sargent (1978; 4 QSOs), Laor et al. (1997ab; 2 QSOs), Neugebauer et al. (1979; 1 QSO) and Schmidt & Green (1983; 6 QSOs). We have used *ROSAT* data to determine the requisite 2-keV flux densities of our QSOs. We obtained count rates from the *ROSAT* All-Sky Survey (RASS; Voges et al. 1999) and pointed observations. All but four of our objects (0043+039, 1004+130, 1259+593, 1700+518) have *ROSAT* detections. Of these four, we note that 0043+039, 1004+130 and 1700+518 were also undetected in moderately deep *ASCA* and *Einstein*

[1] Some authors prefer to work with $\alpha'_{\rm ox}$, the slope of a power law defined by the rest-frame flux densities at 2500 Å and 2 keV. For a 2500 Å to 3000 Å slope of $\alpha_{\rm u}$, we find $\alpha'_{\rm ox} = 1.03\alpha_{\rm ox} - 0.03\alpha_{\rm u}$. Note that $\alpha'_{\rm ox}$, $\alpha_{\rm ox}$ and $\alpha_{\rm u}$ are negative numbers.

observations (Elvis & Fabbiano 1984; Gallagher et al. 1999). We converted the count rates into 2-keV flux densities using a power-law model with Galactic absorption. We used the Galactic column densities from Elvis, Lockman & Wilkes (1989), Lockman & Savage (1995) and Murphy et al. (1996). The power-law energy index ($\alpha_{\rm x}$) was predicted based on a fit to the Hβ FWHM/$\alpha_{\rm x}$ correlation shown in Figure 5a of Laor et al. (1997a): $\alpha_{\rm x} = 6.122 - 1.277\ \log({\rm H}\beta\ {\rm FWHM})$. The H$\beta$ FWHM/$\alpha_{\rm x}$ correlation has been directly established to hold for $\approx 1/4$ of the QSOs in our sample, and our fit is valid for Hβ FWHM in the range $\approx$ 800–11000 km s^{-1}. We excluded 3C 273 from our fit to prevent it from skewing the result due to its small error bar.

The resulting $\alpha_{\rm ox}$ values are given in Table 1, and we show a histogram of these $\alpha_{\rm ox}$ values in Figure 1. For 0043+039 and 1004+130, we were able to place substantially tighter constraints upon $\alpha_{\rm ox}$ using the *ASCA* and *Einstein* results (see above). The $\alpha_{\rm ox}$ distribution is non-Gaussian with $>$ 99% confidence due to its tail towards large negative values of $\alpha_{\rm ox}$. We found acceptable agreement between our $\alpha_{\rm ox}$ values and those for the 23 QSOs given in Table 4 of Laor et al. (1997a). The average absolute difference in $\alpha_{\rm ox}$ for these 23 QSOs is 0.060, and no systematic discrepancies are apparent. We expect any systematic errors to be smaller than the random errors that are inherently present due to the X-ray and optical variability of QSOs. Furthermore, we have verified that none of the main results below depends upon the precise details of how we calculate $\alpha_{\rm ox}$. For example, we recover the same main results if we use $\alpha_{\rm x} = 1.72$ (1.15) for all radio-quiet QSOs (radio-loud QSOs) in the $\alpha_{\rm ox}$ calculation above (see §4.1 of Laor et al. 1997a).

In this paper we have defined a SXW QSO to be a QSO with $\alpha_{\rm ox} \leq -2$. These SXW QSOs thus have 2-keV flux densities that are $\gtrsim 25$ times weaker than expected for a 'normal' QSO (see §4.3 of Laor et al. 1997a). While the precise choice of the $\alpha_{\rm ox}$ division value is somewhat arbitrary, inspection of the histogram shown in Figure 1 indicates that our choice is a reasonable one. The objects with $\alpha_{\rm ox} \leq -2$ stand out clearly from the bulk of the QSO population. We have tested for bimodality of our $\alpha_{\rm ox}$ distribution using the KMM mixture-modeling algorithm described by Ashman, Bird & Zepf (1994, hereafter ABZ94). This algorithm indicates bimodality of the distribution with high statistical significance (the derived KMM P-value is < 0.02; see §2.1 of ABZ94). The algorithm places the 10 QSOs with the largest negative values of $\alpha_{\rm ox}$ into one group (corresponding to $\alpha_{\rm ox} \leq -2$) and the rest of the QSOs into another. The only QSO with an ambiguous KMM classification is 2251+113; this object is discussed further in §6. However, since the KMM algorithm makes several statistical assumptions (e.g., Gaussian-distributed populations; see Hartigan & Hartigan 1985 and ABZ94), we regard our bimodality result as suggestive rather than conclusive. With a sample of 87 QSOs, a distribution with a significant skew tail towards large negative $\alpha_{\rm ox}$ (compare §2 of AT86) could mimic a bimodal one. A nonparametric

Hartigan & Hartigan (1985) dip test is unable to rigorously establish bimodality, but this certainly does not rule out bimodality since the dip test sacrifices a great deal of statistical power for its robustness. The histogram in Figure 1 may be compared with Figure 1 of AT86, although we note that our $\alpha_{\rm ox}$ values are substantially more complete and constraining. Our histogram may also be compared with Figure 10 of Yuan et al. (1998), although in this case our sample is more statistically complete and homogeneous (see §2 of AT86 for a discussion of the importance of complete samples).

We find 10 SXW QSOs among the 87 QSOs in the BG92 sample, and these are listed in Table 2. Thus, SXW QSOs comprise $\approx 11\%$ of the optically selected QSO population. This percentage is in reasonable agreement with the 'detections and bounds' upper limit of AT86. All of our SXW QSOs are radio quiet (with $\log R < 1$) except for 1004+130.[2] In Table 2 we have also given the historical values for $\alpha_{\rm ox}$ from *Einstein* observations (Tananbaum et al. 1986); these values will be used in §8. It is possible that 1259+593 is a SXW QSO as well, but unfortunately the current X-ray data do not allow a tight upper limit to be placed upon $\alpha_{\rm ox}$ for this object ($\alpha_{\rm ox} < -1.75$). We also comment that 0844+349 was seen to be fairly weak in soft X-rays during a *ROSAT* pointed observation but not during the RASS (Yuan et al. 1998). Here we have adopted the RASS count rate, and we discuss this object further in §6.

3. Statistical Analyses of Continuum and Optical Emission-Line Properties

We have performed statistical tests to compare the continuum and optical emission-line properties of SXW QSOs with those of the bulk of the QSO population. In particular, we have compared the properties of our 10 SXW QSOs (hereafter SXW for this group) to those of the other 77 BG92 QSOs (hereafter non-SXW for this group) using two-sample Kolmogorov-Smirnov (hereafter KS) and Kuiper tests (see Press et al. 1992). We chose to apply both of these tests because they statistically complement each other. These tests were objectively chosen in an a priori manner; we did *not* inspect the data in detail and then decide which statistical tests to apply. The main properties we compare are those listed in Tables 1 and 2 of BG92.[3] In addition, we compare the degree of broad-band optical continuum polarization (3200–8600 Å; given in Table 1 of Berriman et al. 1990), the optical continuum slope ($\alpha_{\rm opt}$; given in Table 5 of Neugebauer et al. 1987), and the

---

[2]Here and hereafter we take R to be the ratio of the observed 6 cm and 4400 Å flux densities.

[3]For 1211+143 we have corrected the R parameter following Kellermann et al. (1994). We have also corrected the Hβ FWHM of 1307+085 to be 5320 km s^{-1} and the Hβ shift of 1351+236 to be 1.099.

radio structure (e.g., Miller, Rawlings & Saunders 1993; Kellermann et al. 1994). The probabilities resulting from our KS and Kuiper tests are listed in Table 3, and some of the continuum and optical emission-line properties are illustrated in Figure 2.

3.1. Similarities

In terms of many of their properties, SXW QSOs are homogeneously distributed among the QSO population. For example, there are no statistically significant differences between SXW and non-SXW for M_V, z, or R. Of the 71 BG92 radio-quiet QSOs, 9 are soft X-ray weak. Of the 16 BG92 radio-loud QSOs, 1 is soft X-ray weak (the radio-loud QSO 2251+113 is also quite weak in the soft X-ray band; see §6). These rates of occurrence are statistically consistent according to a Fisher exact probability test for a 2×2 contingency table. In addition, the equivalent width (EW) distributions of Hβ, He II and Fe II are consistent between SXW and non-SXW.

As a class, our SXW QSOs do not show higher broad-band optical continuum polarization than the non-SXW QSOs. Of our 10 SXW QSOs, 9 have broad-band polarization percentages smaller than 0.9%. The one notable exception is 1535+547 which showed the highest polarization percentage in the BQS: 2.5% (see Berriman et al. 1990). We give additional notes on the polarization properties of our SXW QSOs in §5. We also find no evidence for a statistically significant difference between the optical continuum slopes of SXW and non-SXW (i.e. the SXW QSOs do not appear to be systematically redder than the other BG92 QSOs). Although we note that both SXW and non-SXW were drawn from the BQS which employed selection by ultraviolet excess, the range in ultraviolet excess for the BQS is sufficiently large that a real difference would not necessarily be masked.

3.2. Differences

There are several ways in which the optical emission-line properties of SXW QSOs stand out from those of the bulk of the optically selected QSO population. The most notable one is that SXW QSOs systematically have low [O III] luminosities, and we have further illustrated this in Figure 3. In addition, while the Hβ-FWHM and Hβ-asymmetry distributions of SXW and non-SXW are consistent, they have significantly different Hβ-shift and Hβ-shape distributions. The Hβ-shape distributions of SXW and non-SXW are found to be inconsistent by both the KS and Kuiper tests, and SXW QSOs preferentially have 'peaky' line profiles with concave sides. The Hβ-shift distributions of SXW and non-SXW are only shown to be different with high statistical significance by the Kuiper test. This result can be understood by inspection of §14.3 of Press et al. (1992) and Figure 2. The SXW QSOs tend to lie at either the redward or blueward extremes of the Hβ-shift parameter, and this is where the KS test is least sensitive but the Kuiper test is significantly more sensitive (i.e. the KS test is good at finding differences in the median value but not as good at finding differences in the 'spread'). While we must recommend some caution regarding the Hβ-shift result since it is based on only 8 SXW data points (1700+518 and 2112+059 do not have Hβ-shift measurements in BG92 due to their weak [O III] emission), it does appear to be reasonably robust. If we add a hypothetical SXW data point with an Hβ shift of 0, we still find a significant difference between the Hβ-shift distributions of SXW and non-SXW. In this case, the Kuiper test probability is 0.0132.

SXW QSOs tend to lie toward the weak-[O III] end of 'eigenvector 1' as defined by BG92. Eigenvector 1 describes a set of optical emission-line properties that vary together in a highly coordinated manner (e.g., [O III] strength, Fe II strength, Hβ FWHM, and Hβ asymmetry), and it emerged from the Principal Component Analysis (PCA) performed by BG92. Note, however, that eigenvector 1 was derived from a PCA that included $\alpha_{\rm ox}$ (see Table 4 of BG92). In order to be sure that the weak dependence of eigenvector 1 upon $\alpha_{\rm ox}$ is not affecting our result, we have performed our own PCA with $\alpha_{\rm ox}$ excluded. We find that our SXW QSOs still tend to lie at the weak-[O III] end of this '$\alpha_{\rm ox}$-free' eigenvector 1 (see Table 3).

3.3. Radio Structures

The radio structures of SXW and non-SXW are more difficult to compare in a rigorous statistical manner due to the difficulty involved in quantifying radio structure. Our one radio-loud SXW QSO, 1004+130, is lobe dominated, suggesting that we are viewing the active nucleus in a relatively edge-on manner (see Wills, Brandt & Laor 1999 for detailed discussion). There are no obvious radio structure differences between the radio-quiet members of SXW and non-SXW, although we note that better radio imaging data are needed to properly examine this matter. The only radio-quiet SXW QSO with radio structure of particular note is 1700+518. It shows a double source morphology (e.g., see §5.1.3 of Miller et al. 1993 and §3.1 of Kukula et al. 1998).

2251+113 is radio-loud and fairly soft X-ray weak (see §6), and it also is lobe dominated.

4. Ultraviolet Absorption-Line Properties of Soft X-ray Weak QSOs

If photoelectric X-ray absorption is the primary cause of soft X-ray weakness for QSOs, then the X-ray absorbing material might also be detected at other wavelengths. The obvious place to look is in the ultraviolet where cosmically abundant elements have strong bound-bound transitions (e.g., Mathur et al. 1994). Alternatively, X-ray and ultraviolet absorption might have a high frequency of joint occurrence even if the two types of absorption do not arise in the same gas (e.g., Crenshaw et al. 1998 and references therein).

We have therefore collected the available *HST* and *IUE* spectra for the BG92 QSOs to examine if SXW QSOs preferentially show strong ultraviolet absorption. We have focused on absorption in the C IV λ1549 line (hereafter C IV) because the most data are available for this region. There is a wide range in the quality of the spectra, and spectra with particularly poor signal to noise were rejected (see below). Preference was usually given to *HST* data. We found 46 objects with adequate *HST* coverage of at least the C IV region and 9 additional objects with adequate *IUE* coverage. When several datasets were available we co-added them, applying any needed shifts in wavelength scale and weighting appropriately. The rest wavelength scale was determined from a redshift based on the best [O III] λ5007 data where possible.

We have searched all the resulting spectra for BALs or other associated C IV absorption features, and in Table 1 we give our measured rest-frame EWs. All measurements were performed by one author with substantial experience in *HST* and *IUE* data analysis (BJW), and particular effort was made to ensure consistency and uniformity. The measurements were made independently of knowledge of $\alpha_{\rm ox}$. We excluded narrow Galactic interstellar absorption lines based on line identifications over the available spectral range. We were able to confirm some weak C IV absorption features from the doublet wavelength separations or the presence of corresponding absorption features (e.g., N V λ1240, Lyα, O VI λ1034) in the same redshift system. Generally, only measurements with signal to noise greater than 4 were retained. When no absorption was detected we enter 0 for the EW. While our EWs refer to measurable features, they are probably also a reasonable measure of the total EW of C IV associated absorption for a given object. However, we do not give detailed uncertainties. This is because it is difficult to give meaningful limits to any unmeasured associated absorption. Such limits are a complicated function of many parameters: noise, the unknown widths of possible absorption features, the effective continuum placement (especially in the presence of broad emission line wings), and the actual level of the local continuum (which may be low in the true continuum to high near the center of a broad emission line). The archival data are readily accessible to the interested reader, and some examples of spectra are given in §5 and §6.

In Figure 4 we show a plot of $\alpha_{\rm ox}$ versus C IV absorption EW. This plot reveals a striking connection between soft X-ray weakness and strong C IV absorption. Note that the ordinate of this plot spans a range of $\gtrsim 800$ in C IV absorption EW. We have labeled our SXW QSOs and other QSOs of particular interest, and we give object-specific notes on these QSOs in §5 and §6. At least eight of our ten SXW QSOs show C IV absorption with EW > 1 Å, and most have EW > 5 Å. We have performed a Spearman rank-order correlation analysis using the data shown in Figure 4 (including appropriate censoring; Isobe, Feigelson & Nelson 1986) and find the correlation to be significant with > 99% confidence. We have searched for other correlations that could be inducing the correlation of Figure 4 as a secondary effect, and we find none. For example, we do not find any correlation between Hβ FWHM and C IV absorption EW. This correlation is worth checking because $\alpha_{\rm x}$ depends upon Hβ FWHM (see §2); this relationship could have induced a weak dependence of $\alpha_{\rm ox}$ on Hβ FWHM.

In Figure 4 we have also marked bona-fide BAL QSOs with asterisks.[4] These 5 BAL QSOs have the largest C IV absorption EW values in our SXW QSO sample, and inspection of Table 2 reveals that they are also our 5 most optically luminous SXW QSOs. In light of this result, we have used a Spearman analysis to search for a correlation between $M_{\rm V}$ and C IV absorption EW for our 10 SXW QSOs, and we find a correlation that is significant with > 99% confidence. However, with only 8 data points and 2 upper limits we cannot rigorously demonstrate a causative relation between $M_{\rm V}$ and C IV absorption EW for our SXW QSOs.

Finally, we have used a Spearman analysis to search for a correlation between the C IV absorption EW and the broad-band optical continuum polarization (again from Berriman et al. 1990) for our 55 BG92 QSOs with C IV data. The analysis indicates a correlation to be present at the > 96% confidence level, but a plot of these two quantities shows that any correlation has a large scatter.

5. Notes on Individual Soft X-ray Weak QSOs

In this section we give relevant comments on some of our SXW QSOs. In Figure 5 we show spectra of the C IV region for our SXW QSOs, and the reader should refer to this figure while reading this section. 0043+039 and 1700+518 are well-known BAL QSOs that

[4]To be spoken of as a bona-fide BAL QSO, we require a QSO to satisfy the non-zero balnicity requirement outlined in §3.1 of Weymann et al. (1991). To our knowledge, the only BG92 QSOs that clearly satisfy this requirement are 0043+039, 1001+054, 1700+518, 2112+059 and probably 1004+130 (see §5).

have been intensively studied, so we shall not give comments on them here.

1001+054: This QSO was first noted to be soft X-ray weak by Laor et al. (1997), and it has a narrow-line type 1 spectrum. *HST* spectra reveal broad C IV and Lyα absorption, and we measure a small, but non-zero, balnicity index (see Weymann et al. 1991) of ≈ 420 km s^{-1}. A detailed study of the *HST* data will be presented in Wills et al., in preparation.

1004+130 (PKS 1004+130, 4C 13.41): This is the only radio-loud SXW QSO in our sample ($\log R = 2.36$ and the radio spectrum is steep). Its polarization percentage rises with frequency, reaching $\approx 2\%$ by 4000 Å (Antonucci et al. 1996 and references therein). It was first noted to be soft X-ray weak by Elvis & Fabbiano (1984), who studied it using data from *Einstein* and *IUE*. In the low-resolution *IUE* spectra Kinney et al. (1991) recognized unresolved N V and C IV absorption near the emission-line redshift. A high-resolution *HST* GHRS spectrum was obtained by Bowen et al. (1997) to search for intervening absorption by the low-redshift dwarf spheroidal galaxy Leo I. Serendipitously, this spectrum showed the associated N V absorption doublet with at least two velocity components (Figure 3 of Bowen et al. 1997). In this same spectrum, which we retrieved from the *HST* archives, we discovered the corresponding high-ionization absorption lines of the O VI doublet (see Figure 6). These appear to be optically thick and suggest the presence of partial covering. In addition, our detailed analyses of the *IUE* and *HST* data suggest much broader unresolved troughs of C IV, Si IV and O VI, extending to outflow velocities of $\approx 10\,000$ km s^{-1}. We estimate a balnicity index of ≈ 850 km s^{-1} and believe that 1004+130 is probably a low-redshift, radio-loud BAL QSO. There is probable Lyα absorption and strong N V absorption too. This absorption affects the Lyα emission line and accounts for its weakness in this QSO. A detailed analysis of the ultraviolet data is presented by Wills, Brandt & Laor (1999).

1011–040: The archival *IUE* data for this SXW QSO do not reveal any obvious associated absorption, but the spectral quality is not high. It seems unlikely but not impossible that the blue wing of the C IV emission line could be stronger than observed, implying a larger absorption EW. In this case the observed emission line could appear redshifted. However, the peaks of the Lyα and C IV emission lines give a consistent redshift, and the symmetry of the stronger Lyα line does not hint at significant absorption.

1126–041 (Mrk 1298): Wang et al. (1999a) have recently studied the ultraviolet and X-ray absorption in the spectrum of this QSO. *HST* spectra of this object would allow the strong ultraviolet absorption to be studied in significantly more detail.

1411+442: 1411+442 was noted to be soft X-ray weak by Laor et al. (1997), and its ultraviolet absorption and other properties are discussed in detail by Malkan, Green & Hutchings (1987) and Wang et al. (1999b). While its ultraviolet absorption is prominent, it is not a bona-fide BAL QSO. Brinkmann et al. (1999) have presented the *ASCA* data for this QSO, and our independent analysis of these data is in general agreement with theirs. The data suggest absorption by an intrinsic column density of $\approx (1\text{–}2)\times 10^{23}$ cm^{-2}, and there is also evidence for a scattered X-ray component at low energies. The *ASCA* spectrum has limited photon statistics, and the X-ray column density is subject to significant uncertainty because the underlying continuum shape and the ionization state of the X-ray absorber cannot be tightly constrained.

1535+547 (Mrk 486): This object is our weakest detected SXW QSO, and it is also the most highly polarized BQS QSO. Its polarization (2–8%) and associated C IV absorption have recently been studied by Smith et al. (1997), and they argue for a complex broad emission-line region that contains dust. 1535+547 has a narrow-line type 1 spectrum.

2112+059: The *HST* spectrum for this SXW QSO reveals broad ultraviolet absorption by C IV and Lyα (Jannuzi et al. 1998). The broad absorption tends to be shallow, but there are narrower absorption components as well. We measure a balnicity index of ≈ 2980 km s^{-1}. 2112+059 also has an intervening damped Lyα absorption system at $z = 0.2039$ (e.g., Lanzetta, Wolfe & Turnshek 1995), but this system does not materially affect our analysis of the associated ultraviolet absorption. We do not expect this system to cause substantial neutral or ionized X-ray absorption; its neutral hydrogen column density is $\approx 2.5 \times 10^{20}$ cm^{-2}, and we expect any ionized column density to be $\lesssim 5 \times 10^{19}$ cm^{-2}.

2214+139 (Mrk 304): The archival *IUE* spectrum for this SXW QSO does not reveal any obvious associated absorption, but the spectral quality is not high (also see Clavel & Joly 1984). It is not impossible that the blue wing of the C IV emission line could be stronger than it appears, hiding significant absorption. However, the stronger, symmetric Lyα emission line shows no hint of corresponding blueshifted absorption. Rachen et al. (1996) noted that the flatness of the *ROSAT* PSPC spectrum might be due to photoelectric absorption, but detailed spectral analysis of these data is not possible due to the limited photon statistics.

6. Notes on Other Relevant QSOs

Here we give comments on other objects that lie in interesting locations in Figure 4. The reader should refer to this figure while reading this section.

0844+349: Yuan et al. (1998) found 0844+349 to be a SXW QSO during a pointed *ROSAT* observation but not during the RASS. During the pointed observation they found $\alpha'_{\rm ox} = -2.05$ (calculated between 2500 Å and 2 keV). For these data we calculate $\alpha_{\rm ox} = -1.83$ using the methods in §2, and thus 0844+349 does not quite satisfy our criterion for a SXW QSO. This QSO was also not soft X-ray weak during an *Einstein* IPC observation (Kriss 1988). The current data suggest that 0844+349 is not usually a SXW QSO, and it appears to have been caught in an unusually low flux state during the pointed *ROSAT* observation. It has shown soft X-ray variability by a factor of ≈ 6, and this may be due to time-variable X-ray absorption. The poor statistics of the pointed *ROSAT* spectrum make it difficult to examine this issue in detail, especially if significant X-ray scattering is present. Corbin & Boroson (1996) comment that this QSO shows 'associated absorption' in an *HST* spectrum, and our analysis of the *HST* data they used reveals narrow associated Lyα absorption. There are no *HST* data for the C IV region, but co-added *IUE* data suggest C IV absorption consistent in velocity with the Lyα absorption.

1114+445: This QSO shows moderate strength X-ray and ultraviolet absorption by ionized gas (George et al. 1997; Mathur, Wilkes & Elvis 1998). Its intermediate position relative to the low-absorption QSOs and SXW QSOs in Figure 4 is notable. 1114+445 is one of the more highly polarized BQS QSOs (2.3%; Berriman et al. 1990).

1259+593: As noted in §2, this object has only a poor limit on its X-ray flux, and we cannot at present determine if it satisfies our $\alpha_{\rm ox} \leq -2$ criterion to be a SXW QSO. Bahcall et al. (1993) presented an *HST* spectrum for this object, and there is no obvious intrinsic absorption (also see Lu & Zuo 1994). We do not expect significant X-ray absorption from high-velocity cloud Complex C since its neutral hydrogen column density in this direction is $\approx 1.5 \times 10^{20}$ cm^{-2} (see Savage et al. 1993 and references therein). Similarly, UGC 8040 and UGC 8046 should not cause significant X-ray absorption given the ultraviolet constraints on neutral hydrogen absorption lines and the possible ionization levels in the interstellar media of these galaxies (see Bowen et al. 1996 and references therein).

1309+355: This is a flat-spectrum radio-intermediate QSO ($\log R = 1.26$), and Miller et al. (1993) and Falcke et al. (1996) argue that it is a boosted radio-quiet QSO. The radio properties may indicate that the central engine is viewed in a relatively pole-on manner. In light of this, the strong ultraviolet absorption lines seen in the *HST* spectrum (C IV, N V, O VI and Lyα) are notable. This object has $\alpha_{\rm ox} = -1.71$; it is moderately X-ray weak, especially for a radio-loud QSO.

1351+593: This QSO is moderately weak in soft X-rays (also see Elvis 1992), and it shows associated ultraviolet absorption in *HST*, *HUT* and *IUE* spectra (Brosch & Gondhalekar 1984; Granados et al. 1993; Zheng et al. 1999). The absorption runs to fairly high velocities ($\approx$ 3000 km s^{-1}), but 1351+593 probably does not qualify as a bona-fide BAL QSO.

1402+261: This QSO shows moderate strength ultraviolet absorption by Lyα and C IV. The available *ROSAT* data are consistent with no intrinsic X-ray absorption by either neutral or ionized gas (Ulrich-Demoulin & Molendi 1996; Laor et al. 1997).

1404+226: 1404+226 has one of the most extreme narrow-line type 1 spectra for a QSO, and its X-ray spectrum shows a strong soft X-ray excess as well as additional poorly understood complexity (e.g., Ulrich-Demoulin & Molendi 1996; Leighly et al. 1997; Ulrich et al. 1999). The additional complexity may be associated with X-ray absorption edges or lines. *HST* spectra for 1404+226 reveal moderate strength ultraviolet absorption (Ulrich et al. 1999).

1425+267: Laor et al. (1997) pointed out that 1425+267 was moderately soft X-ray weak compared to other radio-loud QSOs, and it has a clear double-lobed radio structure. Complex residuals below 1 keV in archival *ASCA* spectra suggest the presence of intrinsic X-ray absorption, although the absorption cannot be probed in detail due to limited photon statistics. The *HST* spectrum for 1425+267 shows moderate-strength absorption by Lyα and C IV.

1552+085: Turnshek et al. (1997) suggest that this QSO has a C IV BAL in its *IUE* spectrum, but the data are noisy and better spectra are needed to reliably study ultraviolet absorption. For this reason, we do not quote a C IV absorption EW in Table 1, and this object does not appear in Figure 4. We find an $\alpha_{\rm ox}$ value of -1.77, which is fairly small but still somewhat larger than is typically seen for BAL QSOs. 1552+085 is one of the more highly polarized BQS QSOs (1.9%; Berriman et al. 1990).

1704+608 (3C351): This is a lobe-dominated, radio-loud QSO ($\log R = 2.81$) with moderate strength X-ray and ultraviolet absorption by ionized gas (e.g., Mathur et al. 1994; Nicastro et al. 1999). Like 1114+445 and 1425+267, it occupies an intermediate position between low-absorption QSOs and our SXW QSOs (also see Fiore et al. 1994). 1704+608 does not have notable polarization.

2251+113: This steep-spectrum radio-loud QSO ($\log R = 2.56$) is moderately weak in the soft X-ray band, and associated ultraviolet absorption by Lyα, N V, C IV and Si IV has been detected by *HST* (Bahcall et al. 1993). We have analyzed an archival *ASCA* spectrum of this QSO, and these data suggest absorption by an intrinsic column density of $\gtrsim 3 \times 10^{21}$ cm^{-2}. However, as for 1411+442 and 1425+267, the *ASCA* spectrum has limited photon statistics and hence the X-ray column density is subject to significant uncertainty.

7. α_{ox} Correlations after Removal of the Soft X-ray Weak QSOs

We have used our improved α_{ox} values for the BG92 QSOs to examine correlations between α_{ox} and other observables in the most general manner possible. In these correlation analyses, we have excluded our 10 SXW QSOs from consideration. This is important since here we are interested in physical correlations that are not affected by objects where α_{ox} has been altered by strong X-ray absorption (see §8 for the evidence that soft X-ray weakness is primarily due to absorption). We have performed Spearman rank-order correlations between our α_{ox} values and the quantities tabulated by BG92, and our results are given in Table 4. In agreement with Green (1998), we find significant ($P_{\rm Spearman} < 0.04$) correlations between α_{ox} and the EWs of Hβ, [O III], He II and Fe II. In addition, we find the α_{ox} correlations against He II/Hβ, Fe II/Hβ, Hβ FWHM, Hβ asymmetry, α_{opt}, eigenvector 1, eigenvector 2 (see §3.2 of BG92 for discussion), and the 'α_{ox}-free' eigenvector 1 to be significant. The absence of a significant correlation with R is notable. Earlier studies have found a correlation between α_{ox} and R (e.g., Zamorani et al. 1981, hereafter Z81), and this apparent discrepancy is discussed below in §8.2. Our correlations supersede and extend those of BG92 since (1) our α_{ox} values are more complete and constraining than those used by BG92 and (2) we have removed objects with evidence for strong X-ray absorption (see above).

8. Discussion and Conclusions

8.1. The Origin and Demography of Soft X-ray Weak QSOs

We have systematically investigated the nature of the SXW QSOs in the $z < 0.5$ BQS. On the whole, the data support the idea that X-ray absorption is the primary cause of soft X-ray weakness in QSOs. We detect remarkably strong ultraviolet absorption in 8 of our 10 SXW QSOs, and ultraviolet and X-ray absorption have a high probability of joint occurrence. The two SXW QSOs without clear ultraviolet absorption, 1011–040 and 2214+139, both have *IUE* spectra of only limited quality, and *HST* spectra are needed to further examine the possibility of ultraviolet absorption. *ASCA* data are available for only three of our SXW QSOs: 0043+039, 1411+442 and 1700+518. The SXW QSOs 0043+039 and 1700+518 were not detected (consistent with the presence of heavy absorption; see Gallagher et al. 1999), and 1411+442 shows evidence for substantial absorption in its X-ray spectrum (see §5).

Furthermore, we have identified a general correlation between α_{ox} and C IV absorption EW that appears to be due to a continuum of absorption properties (see Figure 4).

Unabsorbed QSOs and SXW QSOs lie towards opposite ends of this correlation, while QSOs with X-ray warm absorbers lie near the middle of the correlation (see the extensive object notes in §5 and §6). BAL QSOs, which comprise a subclass of SXW QSOs, appear to lie at the absorbed extreme of the correlation; the bona-fide BAL QSOs in our SXW QSO sample have ultraviolet absorption that is the strongest we observe, and they often have only upper limits on their X-ray fluxes. The observed correlation is generally consistent with models that postulate a connection between orientation and absorption strength. For example, as one increases the inclination angle one might move through the sequence: unabsorbed QSO, X-ray warm absorber QSO, non-BAL SXW QSO, BAL SXW QSO, and perhaps type 2 QSO. However, our results in §8.2 regarding [O III] luminosity suggest that this picture cannot be complete and that an intrinsic property must also play an important role. In addition, we note that there is evidence suggesting the central engine in the moderately soft X-ray weak QSO 1309+355 is viewed in a relatively pole-on manner (see §6). Finally, the potential relation between $M_{\rm V}$ and C IV absorption EW for our SXW QSOs (see §4) would be difficult to understand in the context of a pure orientation model.

Although the correlation in Figure 4 strongly suggests that soft X-ray weakness is due to absorption, and that the X-ray and ultraviolet absorbers are related, this correlation does not imply that these absorbers are identical. In fact, a uniform screen which completely covers both the X-ray and ultraviolet emission sources is not expected to produce the shape of the correlation seen in Figure 4. This follows since the ultraviolet absorption is by a resonance line, where the absorption EW grows with the absorbing column $N_{\rm H}$ following a 'curve of growth' (e.g., Chapter 14 of Gray 1992), while the X-ray absorption is by bound-free edges, and thus grows like $e^{-\tau_{\rm bf}}$ where $\tau_{\rm bf} \propto N_{\rm H}$. One expects $\alpha_{\rm ox}$ to be practically independent of the C IV EW up to an $N_{\rm H}$ which gives $\tau_{\rm bf} \sim 1$, and above this one expects a very rapid drop in $\alpha_{\rm ox}$ associated with a very slow increase in the C IV EW. Instead, Figure 4 indicates a gradual increase in the C IV EW is associated with a gradual decrease in $\alpha_{\rm ox}$. This may be explained if both the X-ray and ultraviolet absorption are optically thick, but with an absorption covering factor which is less than unity (possibly due to scattering). In this case both $\alpha_{\rm ox}$ and the C IV EW just provide an indication of the X-ray and ultraviolet absorber covering factors, which may vary together.

Other conceivable causes of soft X-ray weakness include (1) an unusual underlying spectral energy distribution and (2) extreme X-ray or optical variability. However, we consider it unlikely that either of these is the primary cause of soft X-ray weakness in optically selected QSOs. Regarding possibility 1, SXW QSOs might be postulated to be intrinsically weak emitters of soft X-rays. Our optical line studies described in §3 allow us to address this since line EWs depend upon the shape of the ionizing spectral energy distribution. We do not, for example, find evidence for a statistically significant difference in the He II EW distributions for SXW QSOs and non-SXW QSOs. The creation of the He II line is driven by 54–150 eV continuum photons, and it would thus be difficult to produce a normal strength line if the underlying spectral energy distribution were anomalously weak in this energy range (see Korista, Ferland & Baldwin 1997 and references therein).

Regarding possibility 2 of the previous paragraph, extreme X-ray variability (with variability amplitude $\gtrsim 10$) has been seen for some BQS QSOs, while such extreme optical variability appears much rarer (e.g., Giveon et al. 1999). To investigate potential $\alpha_{\rm ox}$ variability among our 10 SXW QSO, we have compared our $\alpha_{\rm ox}$ measurements and upper limits with the 3 $\alpha_{\rm ox}$ measurements and 3 $\alpha_{\rm ox}$ upper limits of Tananbaum et al. (1986; see Table 2). While the data are limited, we do not find evidence for outstanding $\alpha_{\rm ox}$ variability.

Our results imply that selection by soft X-ray weakness is an effective ($\gtrsim 80\%$ successful) way to find low-redshift QSOs with strong ultraviolet absorption. This is important from a practical point of view because the optical and X-ray flux densities needed to establish soft X-ray weakness can be obtained in an inexpensive manner from publicly available optical images (e.g., the Palomar Schmidt and UK Schmidt sky surveys) and X-ray data (e.g., the RASS and *ROSAT* pointed observations). When data from the RASS are used, we expect this method to be effective down to about $B = 17$; for (unabsorbed) QSOs with lower optical fluxes, the expected X-ray flux becomes comparable to or less than the RASS sensitivity limit. This selection method appears to be significantly more effective than others that have been developed to find QSOs with strong ultraviolet absorption (e.g., Turnshek et al. 1997).

We have found the percentage of SXW QSOs in the optically selected QSO population (specifically, the $z < 0.5$ BQS) to be $\approx 11\%$. This percentage is in general agreement with previous rough estimates but is more statistically reliable since it is derived from a larger and better-defined sample. We find 4–5 bona-fide BAL QSOs (0043+039, 1001+054, 1700+518, 2112+059 and probably 1004+130) in our sample, and if all BAL QSOs are soft X-ray weak then our methods should have identified all the BAL QSOs in the $z < 0.5$ BQS. It is of interest to examine if the BAL incidence we find is consistent with that found in other QSO surveys (see §11.1 of Krolik 1999). Weymann (1997) gives a BAL QSO incidence of about 11% for the $z = 1.4$–3.0 QSOs from the Large Bright Quasar Survey (LBQS; see Hewett, Foltz & Chaffee 1995), and we would have expected to detect ≈ 9.6 BAL QSOs given this percentage.[5] The number of BALQSOs we detect, while perhaps

[5]We believe the 'true' 11% incidence rather than the 'raw' 8% incidence is the appropriate number to use for comparison in this case (see Weymann 1997). At the wavelengths at which they were selected, the $z < 0.5$ BQS QSOs do not have their fluxes diminished by BAL troughs.

somewhat smaller, does not show any strong inconsistency with the expectation from the LBQS. A Fisher exact probability test for a 2×2 contingency table gives a probability of $\approx 5\%$ when we compare the BQS and LBQS samples. Our results are in general agreement with the idea that the incidence of BALs in modest-redshift QSOs is about the same as in higher-redshift QSOs.

As mentioned in §4, the 5 bona-fide BAL QSOs in our SXW QSO sample are our 5 most optically luminous SXW QSOs. They also have the largest C IV absorption EWs, and among our SXW QSOs we find suggestive evidence for a correlation between $M_{\rm V}$ and C IV absorption EW. If the outflows from our SXW QSOs are optically thick, the C IV absorption EW is expected to be proportional to just the outflow velocity spread and the outflow covering factor, and the outflow velocity spread is plausibly related to the ultraviolet luminosity (e.g., see equation 6 of Scoville & Norman 1995). Thus a relation between $M_{\rm V}$ and C IV absorption EW seems physically plausible, but further work is clearly needed to examine the reality of any relation.

8.2. Interpretation of the Continuum and Optical Emission-Line Analyses

The continuum and optical emission-line analyses discussed in §3 show that SXW QSOs do differ in some respects from non-SXW QSOs. The low [O III] luminosities and EWs of SXW QSOs are striking, and this phenomenon has been previously noted for a subset of SXW QSOs, the low-ionization BAL QSOs (e.g., Boroson & Meyers 1992; Turnshek et al. 1997). If [O III] is an isotropic property, this result suggests that soft X-ray weakness is not merely caused by an orientation effect but arises at least in part as a result of an intrinsic property.[6] A clue to the nature of this property may be found by noting that SXW QSOs also lie toward the weak-[O III] 'negative' end of BG92 eigenvector 1 (see §3).[7] Many of the unabsorbed Seyferts and QSOs with similar values of eigenvector 1 have recently been found to have extreme X-ray spectral and variability properties, and it has been suggested that these 'ultrasoft Narrow-Line Seyfert 1' objects are accreting at relatively high fractions of

[6]Here we are following the line of reasoning discussed in §4.1 of BG92 and §3.2 of Boroson & Meyers (1992). While we recognize that [O III] may have some anisotropy (e.g., see Hes, Barthel & Fobsury 1996; di Serego Alighieri et al. 1997), the best available evidence suggests that this anisotropy is not strong enough to remove the need for an intrinsic property (Kuraszkiewicz et al. 1999a).

[7]Our only SXW QSO with a 'positive' value of eigenvector 1 is the radio-loud QSO 1004+130, and even this object has an unusually small value of eigenvector 1 for a radio-loud QSO. A somewhat similar connection between BAL QSOs and strong optical Fe II emitters has been discussed by Lawrence et al. (1997), although the discussion there was based on qualitative argumentation with a fairly small sample of objects.

the Eddington rate ($\dot{M}/\dot{M}_{\rm Edd}$; e.g., BG92; Boller, Brandt & Fink 1996; Laor et al. 1997a). If an $\dot{M}/\dot{M}_{\rm Edd}$ interpretation of eigenvector 1 is correct, the similar eigenvector 1 values of SXW QSOs would suggest that they also have relatively high $\dot{M}/\dot{M}_{\rm Edd}$. SXW QSOs and ultrasoft Narrow-Line Seyfert 1s would be related objects that differ primarily in the amount of absorption that happens to lie along the line of sight. Accretion at high $\dot{M}/\dot{M}_{\rm Edd}$, where radiation trapping effects are important, is expected to drive substantial mass outflow, and gas in such an outflow could produce the ultraviolet and X-ray absorption observed in SXW QSOs (see §5 of Blandford & Begelman 1999). This gas, perhaps after having cooled, may also have been detected in ultrasoft Narrow-Line Seyfert 1 objects via its emission lines; these objects appear to have especially large amounts of dense gas in their nuclei (e.g., Kuraszkiewicz et al. 1999b; Wills et al. 1999). The significant differences in the Hβ shifts and shapes of SXW QSOs and non-SXW QSOs suggest that either (1) the dynamics of their Broad Line Regions (BLRs) are systematically different, (2) particular parts of their BLRs are preferentially viewed, or (3) broad Hβ absorption near the line peak is modifying the profiles of SXW QSOs (e.g., Anderson 1974). While such effects might plausibly be related to the outflows discussed above, we are at present unable to find a compelling interpretation for the shift and shape differences (this is largely due to the general lack of understanding of the structure and kinematics of the BLR).

The absence of obvious optical continuum reddening, while initially somewhat surprising in light of the ultraviolet and X-ray absorption discussed above, can be understood if the dust in the absorbing gas has been destroyed by sputtering or sublimation. From an empirical point of view, we also note that high-ionization BAL QSOs show only weak reddening despite their strong absorption (e.g., Weymann et al. 1991). The generally low optical continuum polarization of our SXW QSOs may also be understood by analogy with BAL QSOs. While scattering by electrons or dust, together with dust absorption of the central continuum, has been used to explain the high polarization of some BALQSOs, about half of BAL QSOs have polarization percentages $\lesssim 1\%$ (e.g., Schmidt & Hines 1999).

An apparently surprising result from §7 is that $\alpha_{\rm ox}$ does not appear to correlate with R. Earlier studies, in contrast, have found that for a given optical luminosity, the average X-ray emission of radio-loud QSOs is ~ 3 times higher than that of radio-quiet QSOs (e.g., Z81). This apparent discrepancy is due to the following three effects: (1) Z81 define radio-loud QSOs as those having $\log R > 1.88$ rather than $\log R > 1$, (2) Z81 do not detect QSOs with $\alpha_{\rm ox} < -1.75$ (see their Figure 4), and (3) the radio-loud QSOs in Z81 extend up to $\log R \sim 4.8$, while ours have $\log R \lesssim 3$. Figure 5 of Z81 suggests a flattening of $\alpha_{\rm ox}$ with increasing $\log R$, and to make a proper comparison with the BG92 radio-loud QSOs one needs to take subsamples from both samples which follow the same selection criteria. The average $\alpha_{\rm ox}$ for the subsample of 16 QSOs from Table 1 of Z81 with $1 \leq \log R \leq 3$

is $\langle\alpha_{\rm ox}\rangle = -1.48 \pm 0.05$, which is about equal to the Z81 mean for the radio-quiet QSO population (-1.46 ± 0.06) and our mean of the subsample of 14 $\alpha_{\rm ox} > -1.75$ radio-loud QSOs from BG92 (-1.48 ± 0.11). Thus, there is no discrepancy between the Z81 results and our results. The difference in $\alpha_{\rm ox}$ between radio-quiet and radio-loud samples appears to be driven primarily by the radio-loudest ($\log R > 3$) QSOs, which are not present in our sample.

8.3. Future Studies

Systematic hard X-ray spectroscopy of the SXW QSOs discussed in this paper is the obvious next step in the study of these objects. Such spectroscopy should allow determination of the column densities, ionization parameters, and covering factors of the expected X-ray absorbers, and it would let one critically examine the continuum of absorption properties suggested by the $\alpha_{\rm ox}$ versus C IV absorption EW correlation. Furthermore, improved ultraviolet spectra are needed for several of our SXW QSOs. Absorption in species in addition to C IV can constrain physical conditions in the ultraviolet absorber. Objects such as 1011–040 and 2214+139 have only weak limits on C IV absorption and might well show interesting ultraviolet absorption in higher quality spectra. Studies of these two objects will determine whether X-ray weakness in the BG92 QSOs is always associated with ultraviolet absorption, or whether it is possible in some cases to get X-ray absorption without noticeable ultraviolet absorption. Objects such as 1004+130 and 1126–041 also need better spectra to constrain the geometry and dynamics of their known ultraviolet absorption. We are working to obtain the required X-ray and ultraviolet data for our sample.

Finally, the soft X-ray weakness selection method described above may be profitably applied to larger QSO samples.

We thank Th. Boller, M. Elvis, E. Feigelson, J. Nousek, and D. Schneider for helpful discussions. We thank T. Boroson for providing data from BG92. We gratefully acknowledge the support of NASA LTSA grant NAG5-8107 and the Alfred P. Sloan Foundation (WNB), the fund for the promotion of research at the Technion (AL), and NASA LTSA grant NAG5-3431 (BJW).

REFERENCES

Anderson, K. S. 1974, ApJ, 189, 195

Antonucci, R., Geller, R., Goodrich, R. W. & Miller, J. S. 1996, ApJ, 472, 502

Arnaud, K. A. 1996, in Astronomical Data Analysis Software and Systems V: ASP Conference Series 101, ed. Jacoby, G. & Barnes, J. (ASP Press, San Francisco), p. 17

Ashman, K. M., Bird, C. M. & Zepf, S. E. 1994, AJ, 108, 2348

Avni, Y. & Tananbaum, H. 1986, ApJ, 305, 83 (AT86)

Bahcall, J. N. et al. 1993, ApJS, 87, 1

Berriman, G., Schmidt, G. D., West, S. C. & Stockman, H. S. 1990, ApJS, 74, 869

Bevington, P. R. & Robinson, D. K. 1992, Data Reduction and Error Analysis for the Physical Sciences: Second Edition (McGraw Hill, New York)

Blandford, R. D. & Begelman, M. C. 1999, MNRAS, 303, L1

Boller, Th., Brandt, W. N. & Fink, H. 1996, A&A, 305, 53

Boller, Th., Brandt, W. N., Fabian, A. C. & Fink H. 1997, MNRAS, 289, 393

Boroson, T. A. & Green, R. F. 1992, ApJS, 80, 109 (BG92)

Boroson, T. A. & Meyers, K. A. 1992, ApJ, 397, 447

Bowen, D. V., Blades, J. C. & Pettini, M. 1996, ApJ, 464, 141

Bowen, D. V., Tolstoy, E., Ferrara, A., Blades, J. C. & Brinks, E. 1997, ApJ, 478, 530

Brinkmann, W., Wang, T., Matsuoka, M. & Yuan, W. 1999, A&A, in press

Brosch, N. & Gondhalekar, P. M. 1984, A&A, 140, L43

Clavel, J. & Joly, M. 1984, A&A, 131, 87

Corbin, M. R. & Boroson, T. A. 1996, ApJS, 107, 69

Courvoisier, T. J. L. & Paltani, S. 1992, IUE-ULDA Access Guide (ESA Publications, Noordwijk)

Crenshaw, D. M., Maran, S. P. & Mushotzky, R. F. 1998, ApJ, 496, 797

Crenshaw, D. M., Kraemer, S. B., Boggess, A., Maran, S. P., Mushotzky, R. F. & Wu, C. 1999, ApJ, 516, 750

De Bruyn, A. G. & Sargent, W. L. W. 1978, AJ, 83, 1257

di Serego Alighieri, S., Cimatti, A., Fosbury, R. A. E. & Hes, R. 1997, A&A, 328, 510

Elvis, M. 1992, in Frontiers of X-ray Astronomy, ed. Tanaka, Y. & Koyama, K. (Universal Acad. Press, Tokyo), p. 567

Elvis, M. & Fabbiano, G. 1984, ApJ, 280, 91

Elvis, M., Lockman, F. J. & Wilkes, B. J. 1989, AJ, 97, 777

Falcke, H., Patnaik, A. R. & Sherwood W. 1996, ApJ, 473, L13

Fiore, F., Elvis, M., Mathur, S., Wilkes, B. J., McDowell J. C. 1993, ApJ, 415, 129

Gallagher, S. C., Brandt, W. N., Sambruna, R. M., Mathur, S. & Yamasaki, N. 1999, ApJ, 519, 549

George, I. M., Nandra, K., Laor, A., Turner, T. J., Fiore, F., Netzer, H. & Mushotzky, R. F. 1997, ApJ, 491, 508

Giveon, U., Maoz, D., Kaspi, S., Netzer, H. & Smith, P. S. 1999, MNRAS, 306, 637

Goodrich, R. W. 1997, ApJ, 474, 606

Granados, A., Sachs, E., Shull, J. M. & Stocke, J. T. 1993, in The Evolution of Galaxies and Their Environments, ed. Hollenbach, D. J., Thronson, H. A. & Shull, J. M. (NASA Ames Research Center, Moffett Field), p. 115

Gray, D. F. 1992, The Observation and Analysis of Stellar Photospheres (Cambridge University Press, Cambridge)

Green, P. J. 1998, ApJ, 498, 170

Green, P. J. & Mathur, S. 1996, ApJ, 462, 637

Hartigan, J. A. & Hartigan P. M. 1985, Annals of Statistics, 13, 70

Hes, R., Barthel, P. D. & Fosbury, R. A. E. 1996, A&A, 313, 423

Hewett, P. C., Foltz, C. B. & Chaffee, F. H. 1995, AJ, 109, 1498

Isobe, T., Feigelson, E. D. & Nelson, P. I. 1986, ApJ, 306, 490

Jannuzi, B. T. et al. 1998, ApJS, 118, 1

Kellermann, K. I., Sramek, R. A., Schmidt, M., Green, R. F. & Shaffer, D. B. 1994, AJ, 108, 1163

Kinney, A. L., Bohlin, R. C., Blades, J. C. & York, D. G. 1991, ApJS, 75, 645

Korista, K., Ferland, G. & Baldwin, J. 1997, ApJ, 487, 555

Kriss, G. A. 1988, ApJ, 324, 809

Krolik, J. H. & Voit, G. M. 1998, ApJ, 497, L5

Krolik, J. H. 1999, Active Galactic Nuclei. Princeton University Press, Princeton

Kukula, M. J., Dunlop, J. S., Hughes, D. H. & Rawlings, S. 1998, MNRAS, 297, 366

Kuraszkiewicz, J., Wilkes, B. J., Brandt, W. N. & Vestergaard, M. 1999a, ApJ, submitted

Kuraszkiewicz, J., Wilkes, B. J., Czerny, B. & Mathur, S. 1999b, ApJ, in press

Lanzetta, K. M., Wolfe, A. M. & Turnshek, D. A. 1995, ApJ, 440, 435

Laor, A., Fiore, F., Elvis, M., Wilkes, B. J. & McDowell, J. C. 1997a, ApJ, 477, 93

Laor, A., Jannuzi, B. T., Green, R. F. & Boroson, T. A. 1997b, ApJ, 489, 656

Leighly, K. M., Mushotzky, R. F., Nandra, K. & Forster, K. 1997, ApJ, 489, L25

Lockman, F. J. & Savage, B. D. 1995, ApJS, 107, 1

Lu, L. & Zuo, L. 1994, ApJ, 426, 502

Maiolino, R. & Rieke, G. H. 1995, ApJ, 454, 95

Malkan, M. A., Green, R. F. & Hutchings, J. B. 1987, ApJ, 322, 729

Mathur, S., Wilkes, B. J., Elvis, M. & Fiore, F. 1994, ApJ, 434, 493

Mathur, S., Wilkes, B. J. & Elvis, M. 1998, ApJ, 503, L23

Miller, P., Rawlings, S. & Saunders, R. 1993, MNRAS, 263, 425

Murphy, E. M., Lockman, F. J., Laor, A. & Elvis, M. 1996, ApJS, 105, 369

Neugebauer, G., Oke, J. B., Becklin, E. E. & Matthews, K. 1979, ApJ, 230, 79

Neugebauer, G., Green, R. F., Matthews, K., Schmidt, M., Soifer, B. T. & Bennett, J. 1987, ApJS, 63, 615

Nicastro, F., Fiore, F., Perola, G. C. & Elvis, M. 1999, ApJ, 512, 136

Pettini, M. & Boksenberg, A. 1985, ApJ, 294, L73

Press, W. H., Teukolsky, S. A., Vetterling, W. T. & Flannery, B. P. 1992, Numerical Recipes in C: Second Edition. Cambridge University Press, Cambridge

Rachen, J. P., Mannheim, K. & Biermann, P. L. 1996, A&A, 310, 371

Savage, B. D. et al. 1993, ApJ, 413, 116

Schmidt, M. & Green, R. F. 1983, ApJ, 269, 352

Schmidt, G. D. & Hines, D. C. 1999, ApJ, 512, 125

Scoville, N. & Norman, C. 1995, ApJ, 451, 510

Smith, P. S., Schmidt, G. D., Allen, R. G. & Hines, D. C. 1997, ApJ, 488, 202

Tananbaum, H., Avni, Y., Green, R. F., Schmidt, M. & Zamorani, G. 1986, ApJ, 305, 57

Turnshek, D. A. et al. 1994, ApJ, 428, 93

Turnshek, D. A., Monier, E. M., Sirola, C. J. & Espey, B. R. 1997, ApJ, 476, 40

Ulrich-Demoulin, M.-H. & Molendi, S. 1996, ApJ, 457, 77

Ulrich, M.-H., Comastri, A., Komossa, S. & Crane, P. 1999, A&A, in press (astro-ph/9907150)

Véron, P., Mickaelian, A. M., Gonçalves, A. C. & Véron-Cetty M.-P., 1999, in Activity in Galaxies and Related Phenomena, ed. Terzian, Y., Khachikian, E. & Weedman, D. (ASP Press, San Francisco), in press (astro-ph/9809148)

Voges, W. et al. 1999, A&A, in press

Wang, T. G., Brinkmann, W., Wamsteker, W., Yuan, W. & Wang, J. X. 1999a, MNRAS, in press (astro-ph/9903428)

Wang, T. G., Wang, J. X., Brinkmann, W. & Matsuoka, M. 1999b, ApJ, 519, L35

Weymann, R. J. 1997, in Mass Ejection from AGN, ed. Arav, N., Shlosman, I. & Weymann, R. J. (ASP Press: San Francisco), p. 3

Wills, B. J., Laor, A., Brotherton, M. S., Wills, D., Wilkes, B. J., Ferland, G. J. & Shang, Z. 1999, ApJ, 515, L1

Wills, B. J., Brandt, W. N. & Laor, A. 1999, ApJ, 520, L91

Yuan, W., Brinkmann, W., Siebert, J. & Voges, W. 1998, A&A, 330, 108

Zamorani, G. et al. 1981, ApJ, 245, 357 (Z81)

Zheng, W., Kriss, G. A., Espey, B. E. & Davidsen A. F. 1999, in Structure and Kinematics of Quasar Broad Line Regions, ed. Gaskell, C. M., Brandt, W. N., Dietrich, M., Dultzin-Hacyan, D. & Eracleous, M. (ASP Press: San Francisco), in press

---

This preprint was prepared with the AAS LaTeX macros v4.0.

Table 1. $\alpha_{\rm ox}$ and C IV absorption EW values for QSOs in the BG92 sample[1]

PG Name	$\alpha_{\rm ox}$/ C IV EW (Å)	PG Name	$\alpha_{\rm ox}$/ C IV EW (Å)	PG Name	$\alpha_{\rm ox}$/ C IV EW (Å)
0003 + 158	−1.38/0.8	1115 + 407	−1.45/0.4	1425 + 267	−1.63/1.8
0003 + 199	−1.50/0	1116 + 215	−1.57/0.1	1426 + 015	−1.46/0
0007 + 106	−1.43/···[a]	1119 + 120	−1.58/···	1427 + 480	−1.52/0.03
0026 + 129	−1.50/0	1121 + 422	−1.59/0	1435 − 067	−1.63/···
0043 + 039	< −2.00/15.2[b]	1126 − 041	−2.13/5.4	1440 + 356	−1.38/0
0049 + 171	−1.27/···	1149 − 110	−1.42/···	1444 + 407	−1.57/···[a]
0050 + 124	−1.56/0.4	1151 + 117	−1.46/···	1448 + 273	−1.59/···
0052 + 251	−1.37/0	1202 + 281	−1.27/0.4	1501 + 106	−1.64/···
0157 + 001	−1.60/···	1211 + 143	−1.57/0.5	1512 + 370	−1.43/0.2
0804 + 761	−1.52/···	1216 + 069	−1.44/0	1519 + 226	−1.51/···
0838 + 770	−1.54/···	1226 + 023	−1.47/0	1534 + 580	−1.38/···
0844 + 349	−1.54/0.3	1229 + 204	−1.49/0	1535 + 547	−2.45/4.6
0921 + 525	−1.41/···	1244 + 026	−1.60/···	1543 + 489	−1.67/0.4
0923 + 129	−1.41/···	1259 + 593	< −1.75/0	1545 + 210	−1.38/0
0923 + 201	−1.57/···[a]	1302 − 102	−1.58/0	1552 + 085	−1.77/···
0934 + 013	−1.39/···	1307 + 085	−1.52/0	1612 + 261	−1.41/0
0947 + 396	−1.33/0.20	1309 + 355	−1.71/2.8	1613 + 658	−1.21/0
0953 + 414	−1.50/0.17	1310 − 108	−1.52/···	1617 + 175	−1.64/···
1001 + 054	−2.13/12.6	1322 + 659	−1.40/0.2	1626 + 554	−1.37/0
1004 + 130	< −2.01/11.5	1341 + 258	−1.53/···	1700 + 518	< −2.29/84
1011 − 040	−2.01/< 1.2	1351 + 236	−1.52/···	1704 + 608	−1.62/2.4
1012 + 008	−1.66/···	1351 + 640	−1.78/5.7	2112 + 059	−2.11/19
1022 + 519	−1.34/···	1352 + 183	−1.50/0.5	2130 + 099	−1.47/0.8
1048 + 342	−1.52/···	1354 + 213	−1.39/···	2209 + 184	−1.49/···
1048 − 090	−1.41/···	1402 + 261	−1.58/1.2	2214 + 139	−2.02/< 1.2
1049 − 006	−1.56/0.2	1404 + 226	−1.55/1.9	2233 + 134	−1.66/···
1100 + 772	−1.39/0.6	1411 + 442	−2.03/8.5	2251 + 113	−1.86/0.8
1103 − 006	−1.51/0	1415 + 451	−1.51/0	2304 + 042	−1.29/···
1114 + 445	−1.62/3.6	1416 − 129	−1.56/0	2308 + 098	−1.35/0.4

[1] Absorption is considered associated if within −12 000 km s^{-1} of the systemic redshift. We included absorption line strengths beyond −12 000 km s^{-1} only if the absorption appeared to be associated with an absorption complex or BALs. EW values are in the rest frame.

[a] These QSOs have Lyα coverage but no C IV coverage. 0007+106 and 0923+201 have Lyα absorption EWs of 0.5–1.0 Å, while 1444+407 has a Lyα absorption EW of < 0.5 Å.

[b] This value was measured from Figure 10 of Turnshek et al. (1994).

Table 2. SXW QSOs in the BG92 sample

PG Name	z	$M_{\rm V}$	Our $\alpha_{\rm ox}$	Tananbaum et al. (1986) $\alpha_{\rm ox}$[a]
0043+039⋆	0.384	−26.16	< -2.00[b]	⋯
1001+054⋆	0.161	−24.07	−2.13	< -1.78
1004+130⋆[c]	0.240	−25.97	< -2.01[d]	< -1.92
1011–040	0.058	−22.70	−2.01	−1.93
1126–041	0.060	−23.00	−2.13	−1.90
1411+442	0.089	−23.54	−2.03	⋯
1535+547	0.038	−22.15	−2.45	⋯
1700+518⋆	0.292	−26.44	< -2.29	⋯
2112+059⋆	0.466	−27.26	−2.11	< -1.82
2214+139	0.067	−23.39	−2.02	−1.83

⋆The objects 0043+039, 1001+054, 1700+518, 2112+059 and probably 1004+130 are BAL QSOs.

[a]These values were calculated using a power law defined by the rest-frame flux densities at 2500 Å and 2 keV.

[b]This $\alpha_{\rm ox}$ value is from Gallagher et al. (1999).

[c]This is a steep spectrum radio-loud QSO. All the others are radio-quiet QSOs.

[d]This $\alpha_{\rm ox}$ value is from Elvis & Fabbiano (1984).

Table 3. Kolmogorov-Smirnov (KS) and Kuiper test probabilities comparing the continuum and optical emission-line properties of SXW QSOs and non-SXW QSOs

Variable name[a]	KS test probability	Kuiper test probability
$M_{\rm V}$	0.4113	0.1671
$M_{[\rm O\ III]}$	0.0156	0.0091
z	0.9492	0.7500
$\log R$	0.3353	0.8108
EW Hβ	0.7051	0.5711
EW λ5007	0.0324	0.2013
EW λ4686	0.1856	0.6153
EW Fe II	0.1823	0.5901
[O III]/Hβ	0.0959	0.4425
He II/Hβ	0.1856	0.2886
Fe II/Hβ	0.2694	0.6717
FWHM Hβ	0.4902	0.6779
Shift Hβ	0.1205 (80)	0.0032 (80)
Shape Hβ	0.0017	0.0122
Asymmetry Hβ	0.1237	0.5211
$\alpha_{\rm opt}$	0.7998 (74)	0.7442 (74)
Eigenvector 1	0.0012	0.0062
Eigenvector 2	0.1190	0.5088
'$\alpha_{\rm ox}$-free' eigenvector 1	0.0121	0.0195

[a]See BG92 for detailed explanations of these variable names.

[b]Unless noted otherwise, all tests were performed using the 87 BG92 QSOs. When quantities were not available for all 87 BG92 QSOs, we list the number that were used in parentheses after the relevant probability.

Table 4. Spearman rank-order correlations against $\alpha_{\rm ox}$ when our SXW QSOs are removed

Variable name[a]	Spearman R[b]	Spearman probability
$M_{\rm V}$	+0.2268	0.0472
$M_{\rm [O\ III]}$	−0.0268	0.8168
z	−0.1411	0.2207
$\log R$	+0.0915	0.4287
EW Hβ	+0.2653	0.0197
EW λ5007	+0.2525	0.0267
EW λ4686	+0.2884	0.0109
EW Fe II	−0.2968	0.0088
[O III]/Hβ	+0.1424	0.2167
He II/Hβ	+0.2380	0.0371
Fe II/Hβ	−0.3838	0.0006
FWHM Hβ	+0.2392	0.0361
Shift Hβ	−0.0806 (72)	0.5006
Shape Hβ	−0.1638	0.1545
Asymmetry Hβ	−0.3503	0.0018
$\alpha_{\rm opt}$	−0.2954 (65)	0.0169
Eigenvector 1	+0.2917	0.0100
Eigenvector 2	+0.3077	0.0065
'$\alpha_{\rm ox}$-free' eigenvector 1	+0.2408	0.0349

[a]See BG92 for detailed explanations of these variable names.

[b]Unless noted otherwise, all Spearman R values were computed using the 77 non-SXW QSOs. When quantities were not available for all 77 non-SXW QSOs, we list the number that were used in parentheses after the Spearman R value.

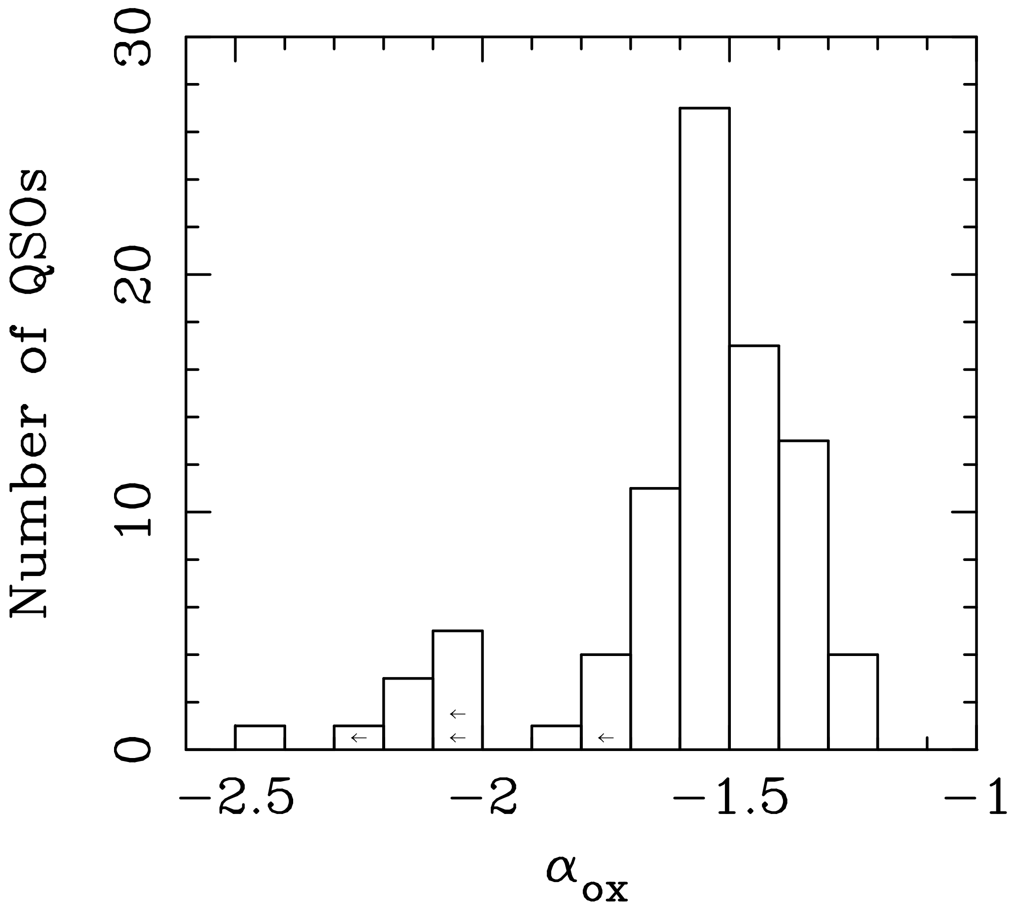

Fig. 1.— Histogram showing the $\alpha_{\rm ox}$ distribution of the 87 BG92 QSOs. The values of $\alpha_{\rm ox}$ refer to the positions indicated by the longer tick marks on the top axis. The four nondetections present in this histogram (0043+039, 1004+130, 1259+593 and 1700+518) are labeled with left-pointing arrows.

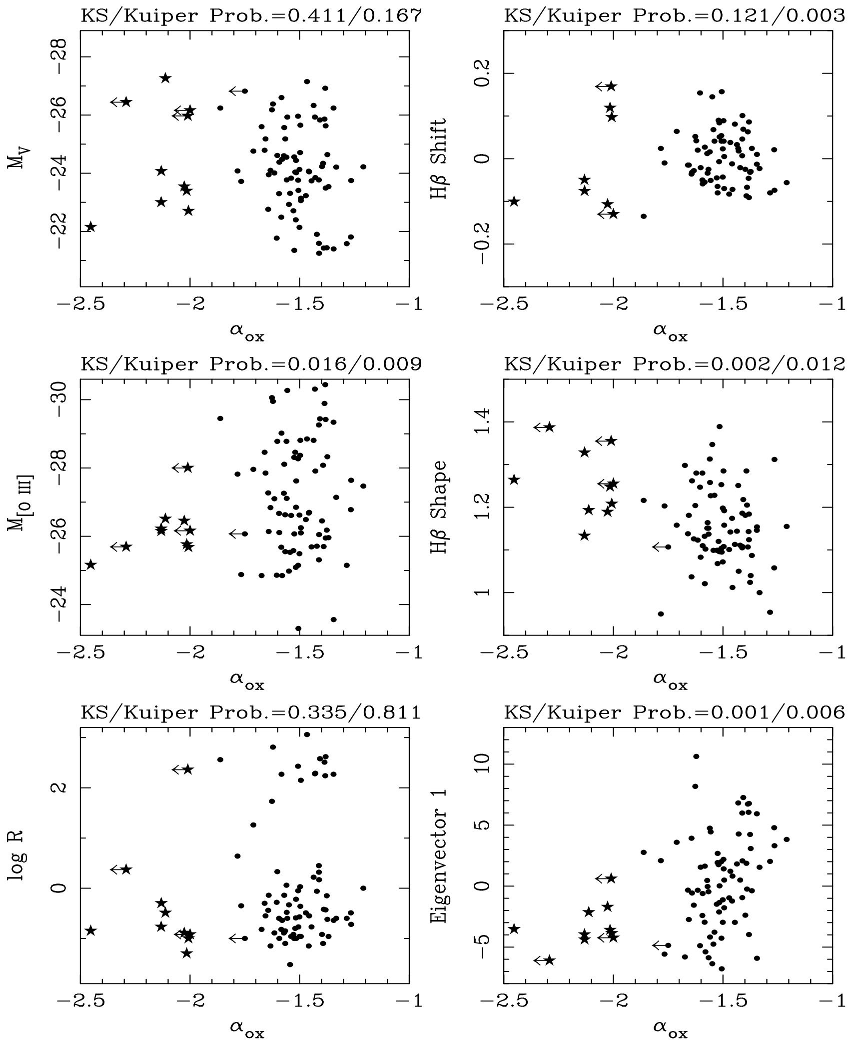

Fig. 2.— Comparisons of the continuum and optical emission-line properties of our 10 SXW QSOs (stars, referred to as SXW in the text) to the other 77 BG92 QSOs (dots, referred to as non-SXW in the text). We do not show plots for all the properties discussed in the text but rather focus on the most germane ones. Above each panel are listed the Kolmogorov-Smirnov (KS) and Kuiper test probabilities that the stars and dots are drawn from the same distribution. Note that the two samples are consistent with being drawn from the same $M_{\rm V}$ and $\log R$ distributions but that the SXW QSOs differ in terms of the other illustrated properties.

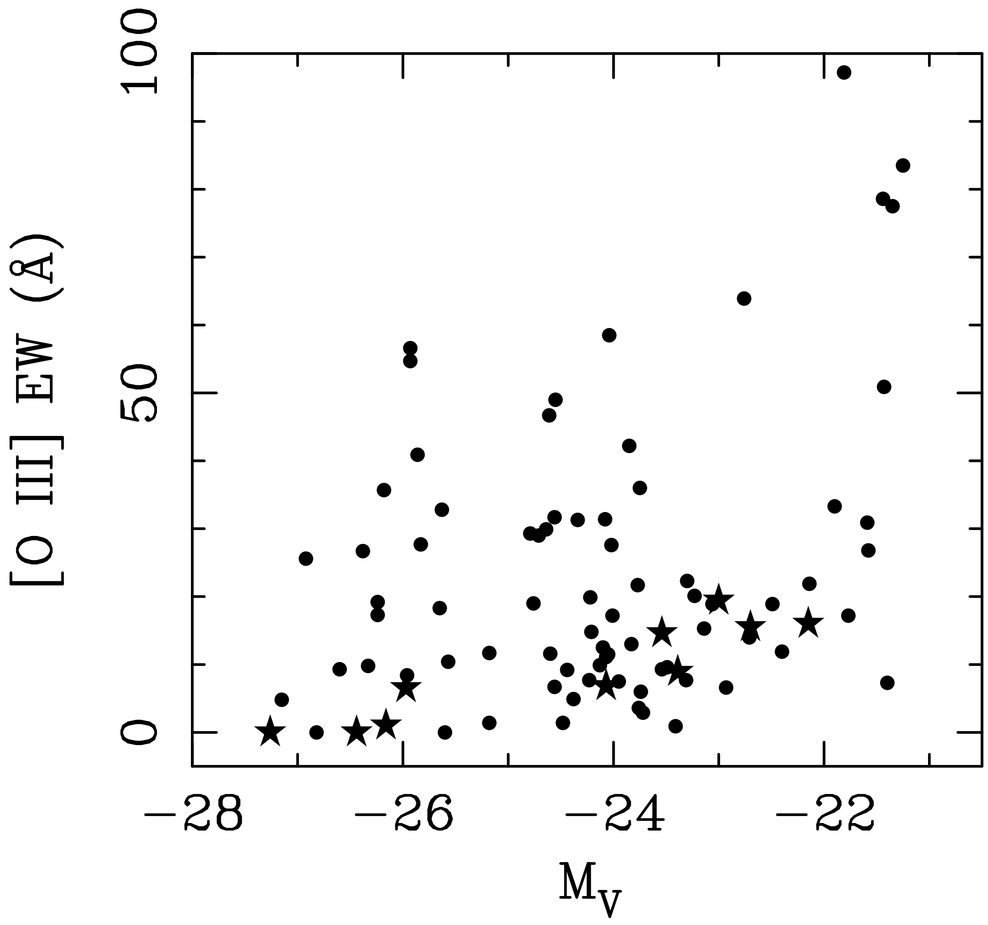

Fig. 3.— Plot of [O III] EW versus $M_{\rm V}$ for the BG92 QSOs. Stars show our 10 SXW QSOs, and dots show the other BG92 QSOs. Note that the SXW QSOs have systematically low [O III] EWs. The point for 1612+261 lies outside the boundary of this plot at $M_{\rm V} = -23.77$, [O III] EW = 157 Å.

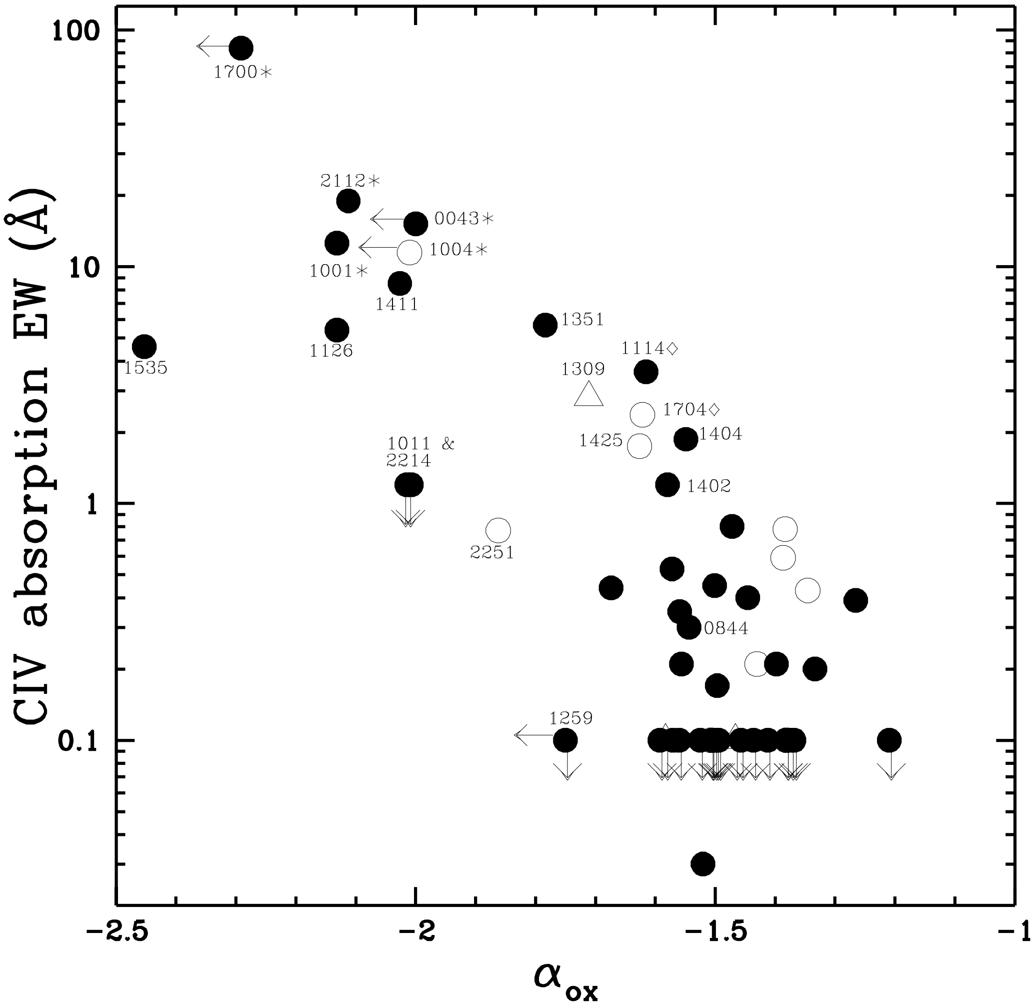

Fig. 4.— Plot of $\alpha_{\rm ox}$ versus C IV absorption-line EW (in the rest frame) for the BG92 QSOs. Following BG92, solid dots are radio-quiet QSOs, open triangles are core-dominated radio-loud QSOs, and open circles are lobe-dominated radio-loud QSOs. SXW QSOs and other particularly relevant objects are labeled by the right ascension part of their BQS name. An asterisk (∗) to the right of an object's name indicates that it is a BAL QSO or probable BAL QSO (see §5 for further discussion), and a diamond (◇) to the right of an object's name indicates that it is known to have an X-ray warm absorber. We have assigned an EW of < 0.1 Å when no C IV absorption was detected.

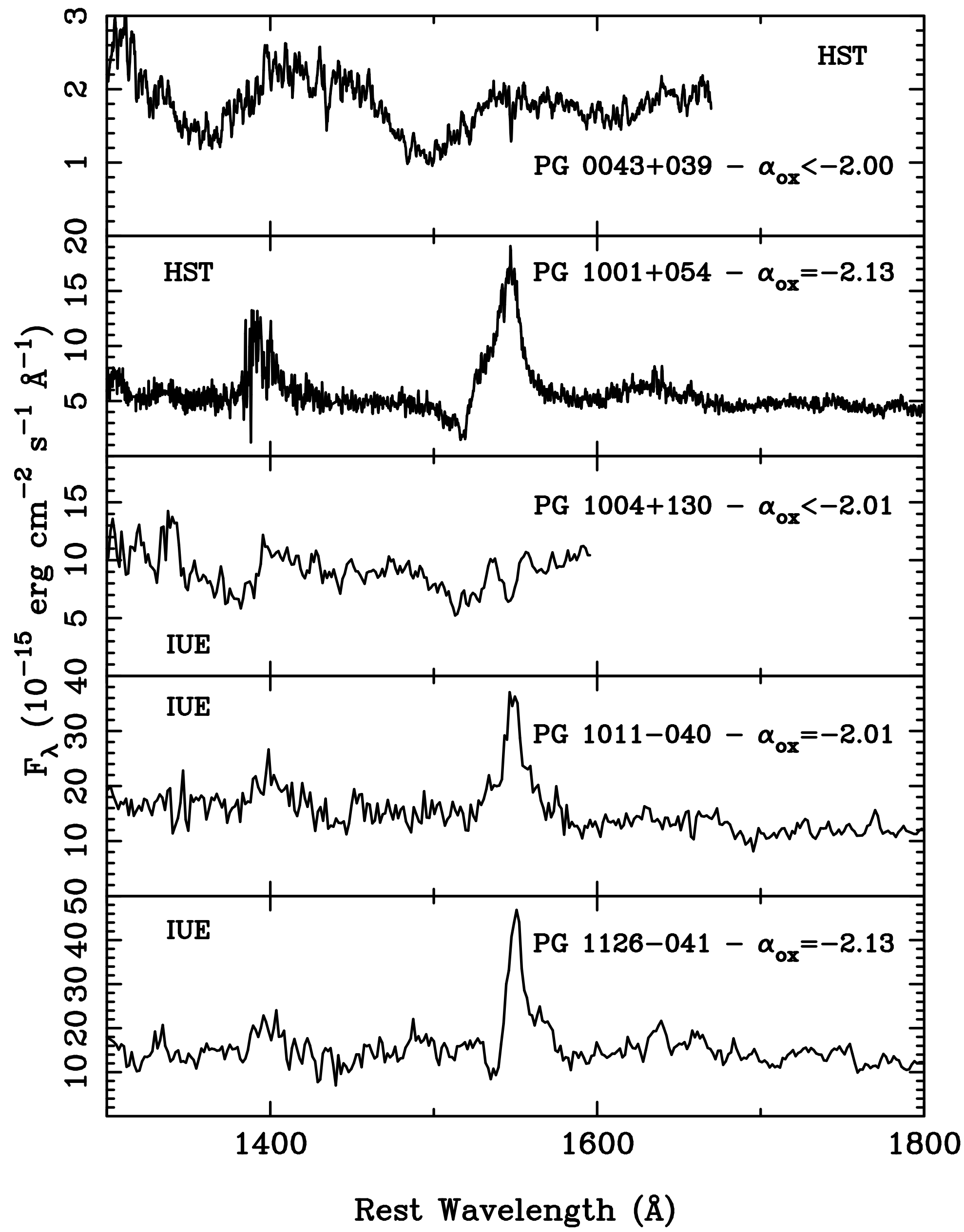

Fig. 5.— Spectra of the regions of the broad C IV emission line for our ten SXW QSOs. Note the strong, blueshifted C IV absorption seen in most spectra. In each panel we also give the α_{ox} value and the name of the satellite that took the data shown.

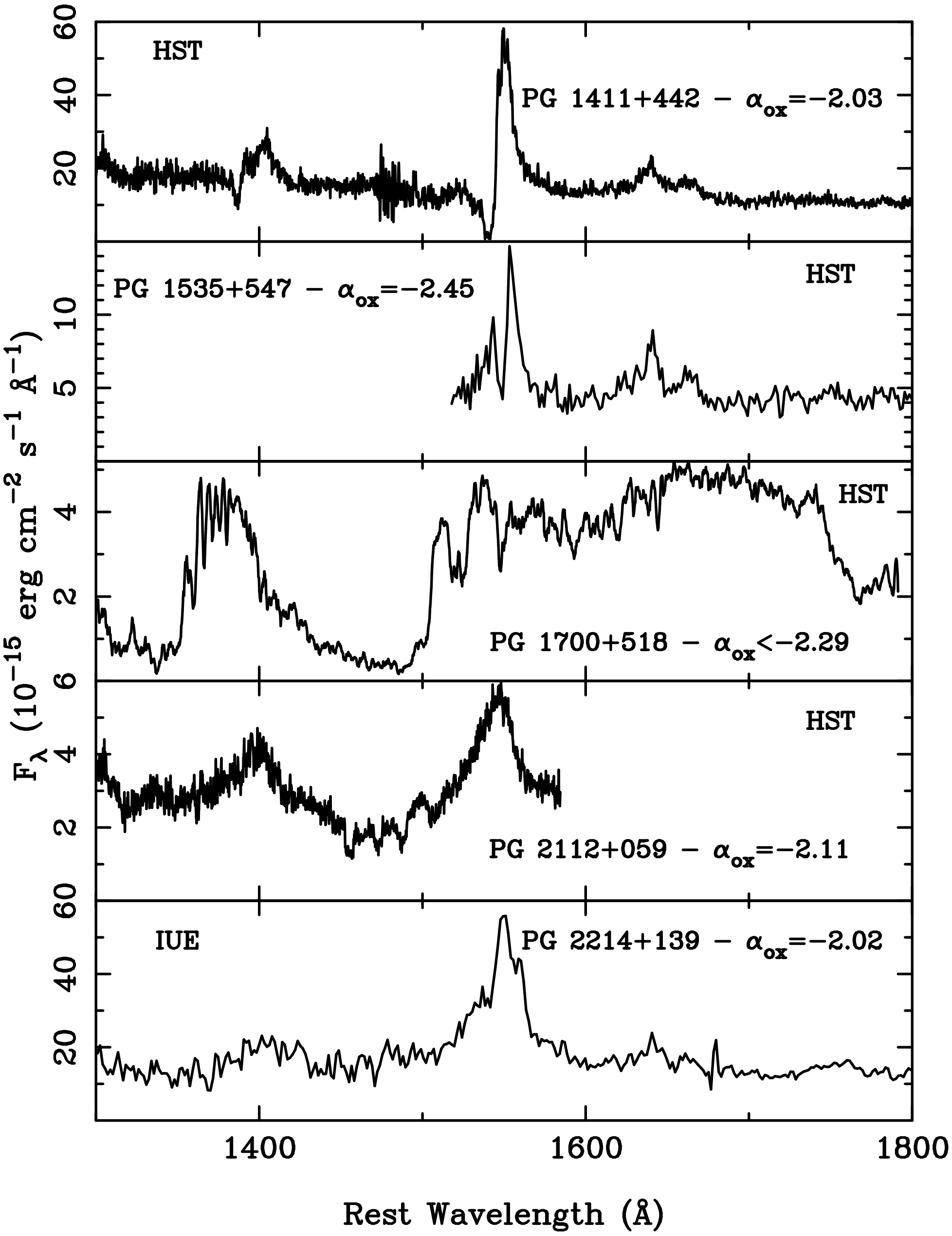
HST
PG 1411+442 – α_{ox}=−2.03
PG 1535+547 – α_{ox}=−2.45
HST
HST
PG 1700+518 – α_{ox}<−2.29
HST
PG 2112+059 – α_{ox}=−2.11
IUE
PG 2214+139 – α_{ox}=−2.02
F_λ (10^{-15} erg cm^{-2} s^{-1} Å^{-1})
Rest Wavelength (Å)
1400
1600
1800

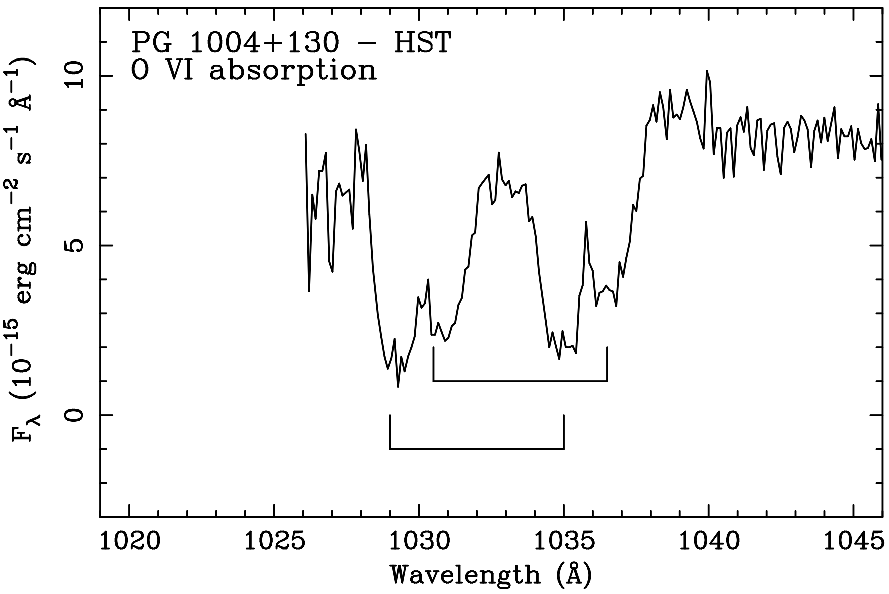

Fig. 6.— Archival *HST* GHRS spectrum showing the strong O VI absorption present in the ultraviolet spectrum of 1004+130. Two absorption systems are seen at $z = 0.2364$ and $z = 0.2387$.